Article

Pressure-Induced Superconductivity of the Quasi-One-Dimensional Organic Conductor (TMTTF)$_2$TaF$_6$

Miho Itoi [1,*] **, Toshikazu Nakamura** [2] **and Yoshiya Uwatoko** [3]

[1] Physics Section, Division of Natural Sciences, Nihon University School of Medicine, Itabashi 173-8610, Japan
[2] Institute for Molecular Science, Okazaki 444-8585, Japan; t-nk@ims.ac.jp
[3] Institute for Solid State Physics, The University of Tokyo, Kashiwa 277-8581, Japan;
    uwatoko@issp.u-tokyo.ac.jp
[*] Correspondence: itoi.miho@nihon-u.ac.jp

Abstract: We investigated the superconductivity of (TMTTF)$_2$TaF$_6$ (TMTTF: tetramethyl-tetrathiafulvalene) by conducting resistivity measurements under high pressure up to 8 GPa. A cubic anvil cell (CAC) pressure generator, which can produce hydrostatic high-pressure, was used for this study. Since the generalized temperature-pressure (*T-P*) diagram of (TMTCF)$_2$X (C = Se, S, X: monovalent anion) based on (TMTTF)$_2$PF$_6$ (T_{CO} = 70 K and spin-Peierls: SP, T_{SP} = 15 K) was proposed by Jérome, exploring superconductivity states using high-pressure measurement beyond 4 GPa has been required to confirm the universality of the electron-correlation variation under pressure in (TMTTF)$_2$X (TMTTF)$_2$TaF$_6$, which has the largest octahedral-symmetry counter anion TaF$_6$ in the (TMTTF)$_2$X series, possesses the highest charge-ordering (CO) transition temperature (T_{CO} = 175 K) in (TMTTF)$_2$X and demonstrates an anti-ferromagnetic transition (T_{AF} = 9 K) at ambient pressure. A superconducting state in (TMTTF)$_2$TaF$_6$ emerged after a metal-insulator transition was suppressed with increasing external pressure. We discovered a superconducting state in $5 \leq P \leq 6$ GPa from T_c = 2.1 K to 2.8 K, whose pressure range is one-third narrower than that of X = SbF$_6$ ($5.4 \leq P \leq 9$ GPa). In addition, when the pressures with maximum SC temperatures are compared between the PF$_6$ and the TaF$_6$ salts, we found that (TMTTF)$_2$TaF$_6$ has a 0.75 GPa on the negative pressure side in the *T-P* phase diagram of (TMTTF)$_2$PF$_6$.

Keywords: one-dimensional organic conductor; superconductivity; high-pressure measurement

1. Introduction

Since the discovery of the first organic superconductivity in (TMTSF)$_2$PF$_6$ (tetramethyl-tetraselenafulvalene-hexafluorophosphate), quasi-one-dimensional (Q1D) organic conductors (TMTCF)$_2$X (C = Se and S, X = monovalent anion) have been extensively investigated because electronic-correlations related to spin, charge, and dimensionality generate various types of ground states [1–5]. In the (TMTCF)$_2$X crystal, face-to-face TMTCF molecules align perpendicularly along the *a*-axis. The hybridization of p-electrons on Se or S atoms in the TMTCF molecules leads to strong one-dimensional conductivity, and the 1D-TMTCF chain is well-separated by the monovalent anion X layer. The (TMTCF)$_2$X system has a 3/4 filling band structure [6]. Their flexible-molecular packing consequently produces multihued ground states, which change from AFM (anti-ferromagnetism) I-SP (spin-Peierls), AFM II (commensurate SDW), and incommensurate SDW (spin density wave) to an SC (superconductivity) phase at low temperatures, by controlling the superposed electron density in both inter-and intra-chains using chemical and the applied pressures [1]. For more than three decades, the generalized phase diagram has been extended by efforts in synthesizing TMTTF salts with *centrosymmetric* (*cs*) (X = Br, I, PF$_6$, AsF$_6$, SbF$_6$, NbF$_6$, and TaF$_6$) and *non-centrosymmetric* (*ncs*) anions (X = BF$_4$, ClO$_4$ and ReO$_4$). Simultaneously, many scientists have attempted to clarify the ground state changes of (TMTTF)$_2$X by conducting pressure measurements, and the validity of the temperature-pressure (*T-P*) diagram corresponding

between the chemical pressure and the external pressure has been confirmed. In particular, the high-pressure investigation exceeding 4 GPa has revealed the existence of the superconductivity phase in the (TMTTF)$_2$X series [2,3,7–10].

The emergence of the superconducting phase in the (TMTTF)$_2$X series is understood as a crossing over anti-ferromagnetic fluctuation. (TMTTF)$_2$Br is the first superconductor in TMTTF series (T_C = 0.8 K@ 2.6 GPa) [11], whose ground state shifts from AFM II (T_{AF} = 15 K, C-SDW: commensurate) to SDW (I-SDW: incommensurate) by external pressure [12–14]. The SDW transition temperature decreases due to the imperfect nesting of Fermi surfaces by applying external pressure. The SDW phases observed in (TMTSF)$_2$MF$_6$ (M = P, As, Sb) were explained by the electron correlation and two-dimensionality with mean-field theory [15]. As it stands that the SC phase in (TMTCF)$_2$X always neighbors the SDW, there are many reports about the exotic superconductivity properties of (TMTCF)$_2$X, for instance, the anisotropic SC revealed by high magnetic field measurements [16,17] and by muon spin rotation [18].

The charge-ordering (CO) state was observed in the (TMTTF)$_2$X series, except for (TMTTF)$_2$ClO$_4$, (TMTTF)$_2$SCN, and (TMTTF)$_2$I [19–21]. The CO transition of (TMTTF)$_2$X is called a structureless transition since only a small change in the dimer position was observed by X-ray diffraction measurement [22]. The spatial charge disproportion on TMTTF molecules affects the spin state at low temperatures. In the case of (TMTTF)$_2$X, which has an octahedron symmetry counter anion, the X = PF$_6$ and AsF$_6$ salts go into the SP phase from the CO phase, while the X = SbF$_6$, NbF$_6$ [23], and TaF$_6$ salts change to AFM I phase by cooling, depending on the CO pattern, dimensionality, and spin fluctuation [24,25]. Below 3 GPa pressure region, ^{13}C NMR studies in X = SbF$_6$ have revealed that the ground states vary from AFM I → spin gap → AFM II (C-SDW) (Figure 1) [26,27]. The ground state change from SDW to SC became decisive through the high-pressure resistivity measurement up to 10 GPa using a cubic anvil cell (CAC); the superconducting phase of (TMTTF)$_2$SbF$_6$ was observed as an anomalously wide pressure range (5.4 < P < 9 GPa) under limited temperature above 1.8 K [9].

(TMTTF)$_2$TaF$_6$ has the largest cell volume in the (TMTCF)$_2$X series, with a cs anion. The one-dimensional character was confirmed by the result of the single-crystal X-ray diffraction analysis [28]. To understand the electron correlation, confirmations of the existence of the SC state and the pressure-dependent ground-state change toward the SC state in (TMTTF)$_2$TaF$_6$ are necessary. In this paper, we investigated the resistivity behaviors of (TMTTF)$_2$TaF$_6$ under high pressures up to 8 GPa and compared it to those for other TMTTF compounds (X = PF$_6$, AsF$_6$, and SbF$_6$).

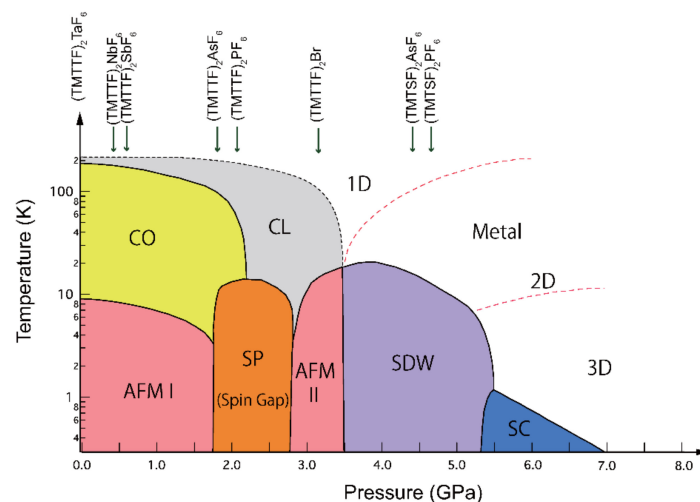**Figure 1.** Electronic temperature-pressure (*T-P*) diagram for quasi-one-dimensional (Q1D) organic conductors (TMTCF)$_2$X (C = S and Se), which start from the ground state of the (TMTTF)$_2$TaF$_6$ salt

(CO state T_{CO} = 175 K and AFM T_{AF} = 9 K), suggested by Dressel et al. and Oka et al. This *T-P* diagram is depicted from the references [5,23,26,27,29–32]. The generalized *T-P* diagram (i.e., generalized electron correlation diagram) of $(TMTCF)_2X$ was first established by D. Jérome and coworkers in 1991 [1]. The abbreviations for described states in the diagram are CO (charge-ordering state), CL (charge-localized state), SP (spin-Peierls state), AFM (anti-ferromagnet, I: commensurate state, II: commensurate SDW), SDW (spin density wave), and SC (superconducting state).

2. Experimental Section

The sample preparation of $(TMTTF)_2TaF_6$ was detailed in Ref. [28]. The single crystal $(TMTTF)_2TaF_6$ is a black needle type; the sample size used for resistivity measurement was 800 μm × 15 μm × 10 μm. The high-pressure resistivity measurement was performed by using a CAC apparatus at the Institute for Solid State Physics (ISSP), The University of Tokyo. The resistivity of $(TMTTF)_2TaF_6$ was measured along the *a*-axis (crystal growing direction) by a conventional four-probe method. The four Au electric terminals (φ 10 μm Au wire) were in contact with carbon paste on the sample surface and the ends of Au wires were relayed to φ 15 μm Pt wires with Au paste to avoid wire cutting during the application of high pressures. The four relayed Pt wires are fixed with a small piece of paper by using epoxide resin adhesives to prevent sample breaking by the shock when the high pressure was applied. The sample with electrodes was sealed in a small Teflon cell (φ 2.0 mm) with the pressure medium Fluorinert 70:77 (1:1) mixture and then wrapped with a cubic MgO gasket (6 mm squares), which also served as the second pressure medium. The four Pt electric leads outside of the Teflon cell were wired with thin Au ribbons on the MgO gasket. The MgO gasket was isotopically compressed up to 250 tons by Tungsten carbide anvils, which also play a role in four-wire electronic contact materials. The CAC can generate a high-quality steady hydrostatic pressure by controlling a constant load system up to 12 GPa. The temperature range for this measurement was from 1.8 K to 295 K and the resistance value of $(TMTTF)_2TaF_6$ was recorded upon heating. External pressure was applied on $(TMTTF)_2TaF_6$ between 0 GPa and 1.4 GPa; the resistance varied due to unsteady attachment between the gasket and CAC anvils. At 1.5 GPa, the MgO gasket was compressed enough to achieve steady resistance of the TaF_6 salt. Therefore, we did not measure the resistivity at 0 GPa; the measurement starts from 1.5 GPa. The resistivity along the *a*-axis was normalized by using the length and the surface values at room temperature.

3. Results and Discussion

At ambient pressure, the CO phase transition temperature (T_{CO} = 175 K) of *X* = TaF_6 is the highest in the TMTTF series with octahedron monovalent anion. The CO transition temperature increases with increasing the octahedron anion size, PF_6 (70 K), AsF_6 (102 K) SbF_6 (154 K), and NbF_6 (165 K) [23]. The stoichiometry-controlled salt $(TMTTF)_2[AsF_6]_{1-x}[SbF_6]_x$ ($x\sim0.3$) has a higher T_{CO} of 120 K, which is between the temperatures of the AsF_6 and SbF_6 salts, and the characteristic SP magnetic susceptibility behavior is suppressed at a low temperature [33]. It was reported that the transition between SP and AFM I states occurs at $x\sim0.5$ chemical pressure [34], while the pressure experiment on $(TMTTF)_2SbF_6$ revealed that the AFM I state changed to a spin gap state due to the external pressure of 0.5 GPa, and the CO state becomes unclear above 0.5 GPa. [26]. (More details for the pressure effect on the CO state in *X* = AsF_6 and SbF_6 are in Ref [35]). The CO state in the TaF_6 salt has a -O-o-O-o- pattern (O: charge-rich site, o: charge-poor site) as in the SbF_6 salt, which coexists in the AFM I phase at ambient pressure [27,32]. The temperature-dependent magnetic susceptibility shows a characteristic one-dimensional decrease from 300 K to 50 K, and a rapid decrease was observed around 30 K. $(TMTTF)_2TaF_6$ undergoes an anti-ferromagnetic transition at 9 K [27].

Figure 2a shows the temperature-dependent resistivity of $(TMTTF)_2TaF_6$ in the *a*-axis direction under pressures from 1.5 GPa to 8 GPa. For the measurement, the initial temperature was set to around 1.8 K by cooling from room temperature, and then the temperature was gradually heated. Generally, the metallic conductivity of the TMTTF

series becomes unstable due to the charge localization at T_ρ in the high-temperature region. For the TaF$_6$ salt, T_ρ is reported as ~200 K, which is quite close to T_{CO} = 175 K. The resistivity at room temperature is 0.1 $\Omega\cdot$cm [32]. In the case of our pressure measurement, the resistivity at 1.5 GPa was 0.35 $\Omega\cdot$cm at room temperature, whose value was two orders higher than that (0.005 $\Omega\cdot$cm) of (TMTTF)$_2$SbF$_6$ (Figure 2b). A possible cause of the high resistivity value at 1.5 GPa is considered as a partial remnant charge localization caused by interfering with smooth volume compression and/or exceeding the anisotropic crystal deformation by a large TaF$_6$ anion under low pressures.

Figure 3a shows the resistivity value at 290 K under several pressures for (TMTTF)$_2$X (X = PF$_6$, AsF$_6$, SbF$_6$, and TaF$_6$) by using the CAC pressure generator. The pressure-dependent resistivities of X = PF$_6$, AsF$_6$, and SbF$_6$ were plotted with the data in Refs. [7–9]. The resistivity rapidly decreases up to 5 GPa and the value becomes almost unchanged beyond 6 GPa, although the resistivities for (TMTTF)$_2$X (PF$_6$, AsF$_6$, and SbF$_6$) are almost suppressed below 2 GPa (Figure 3a inset). It should be noted that the resistivity of the SbF$_6$ salt is the lowest in the (TMTTF)$_2$X series from 1.5 GPa to 10 GPa.

For the resistivity of the TaF$_6$ salt at 1.5 GPa, we observed the drastic resistivity drop up to 100 K upon heating. After the temperature reached 100 K, the resistivity has a gradual incline (Figure 2b). The activation energies of Δ_ρ and Δ_S were obtained from a simple formula, $\log \rho(T) = \frac{\Delta}{T} + \log \rho_0$. The inclination changes at a higher temperature and a second inclination change at a lower temperature correspond to T_ρ and T_S in Figure 2c, in $\log \rho(T)$-1/T plot. Here, the sample size reduction caused by thermal expansion and pressure effects is not taken into account for the $\log \rho(T)$ calculation. Figure 3b,c show the pressure-dependent activation energies (Δ_ρ and Δ_S) for (TMTTF)$_2$X (X = PF$_6$, AsF$_6$, SbF$_6$ and TaF$_6$). It should be noted that the Δ_ρ value in Figure 3b includes both activation energies coming from CO and Mott localization. The CO gap Δ_{CO} has been discussed in several reports by resistivity measurements [20,32,33], using the formula $\Delta_{CO} = \sqrt{\Delta(T)^2 - \Delta^2(T_{CO})}$ (here $\Delta(T) = T \ln \rho$ in the CO state and $\Delta^2(T_{CO})$ is the value above T_{CO}). Each Δ_{CO} gap at ambient pressure is ~560 K for TaF$_6$, ~500 K for SbF$_6$, 430 K for [AsF$_{61-x}$[SbF$_{6x}$ (x ~0.3), ~315 K for AsF$_6$, and ~217 K for PF$_6$, which increases proportionally to T_{CO} [32,33]. Δ_{CO} values are less than half of the obtained Δ_ρ values at 0 GPa and the order of magnitude of (TMTTF)$_2$X is Δ_ρ (SbF$_6$) > Δ_ρ (AsF$_6$) > Δ_ρ (PF$_6$), which is different from Δ_{co} (TaF$_6$) > Δ_{co} (SbF$_6$) > Δ_{co} (AsF$_6$) > Δ_{co} (PF$_6$). For the obtained data of high-pressure measurements for the TaF$_6$ salt, the extraction of the Δ_{CO} value at around 1.5 GPa is already unresolved due to an unclear transition at T_{CO}.

The Δ_ρ and Δ_S at 1.5 GPa for (TMTTF)$_2$TaF$_6$ are 117 K (T_ρ~90 K) and 116 K (T_S~20 K), respectively, which correspond to the values at about 2.1 GPa and 1.5 GPa for those of (TMTTF)$_2$SbF$_6$, respectively. The Δ_ρ becomes comparable to those of other (TMTTF)$_2$X salts near 2.0 GPa since the CO state of the TaF$_6$ salt already vanishes, then Δ_ρ values coincide with almost constant values in (TMTTF)$_2$X salts above 3 GPa. Meanwhile, activation energy Δ_S corresponds to a spin-related transition (SP, AFM II, and SDW), according to the similar analysis of (TMTTF)$_2$X [2,3,7–9]. With increasing applied pressures, high resistivity at low temperatures dramatically drops and the metallic behavior becomes dominant above 40 K upon heating (see Figure 2b). At 3 GPa, the resistivity at room temperature still shows a high value of 0.3565 $\Omega\cdot$cm; the minimum drop in the resistivity curve appears at around 20 K in the resistivity-temperature curve, written in both logarithmic axes. The respective activation energies Δ_S at 3 GPa and 4 GPa are 22 K (T_S = 13 K) and 10 K (T_S = 8 K), respectively, which correspond to the activation energies observed in the X = SbF$_6$ salt at ~4.6 GPa and 5.3 GPa, respectively (see Figure 3c). It should be noted that the AFM II (C-SDW) and SDW (I-SDW) transition temperatures are ~15 K (at $0 \leq P < 0.3$ GPa) and ~23 K (at $0.3 < P \leq 0.75$ GPa) in (TMTTF)$_2$Br [12]. Here, the resistivity of the TaF$_6$ salt between 200 K and 300 K at 4 GPa becomes almost equal to that of X = SbF$_6$ at room temperature (see Figure 2b).
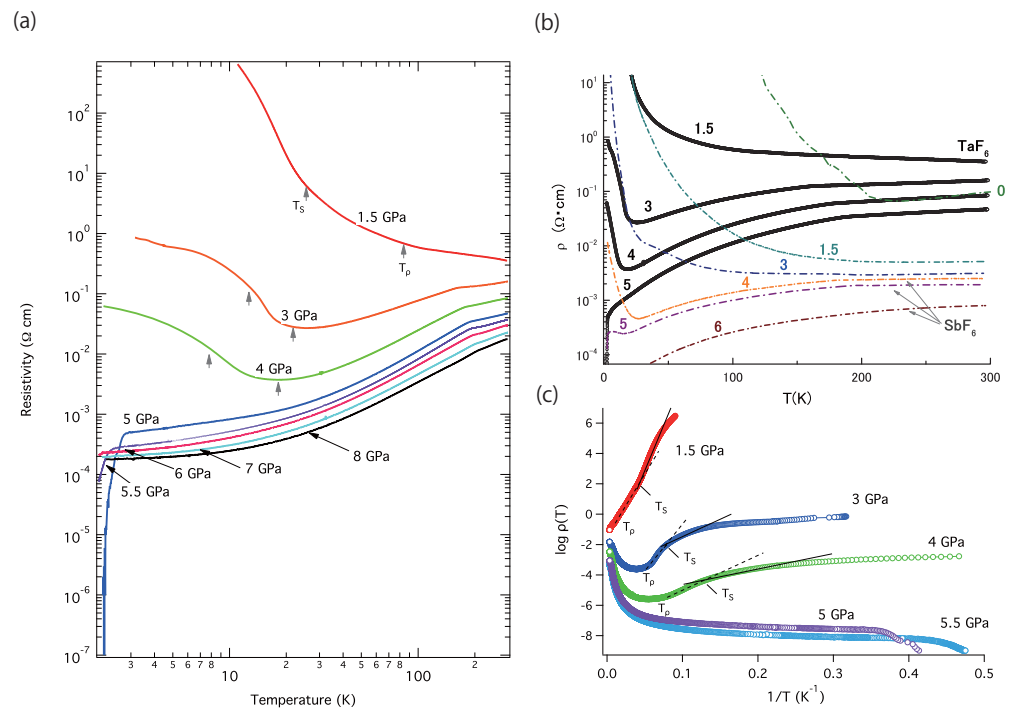
Figure 2. (**a**) Temperature dependence of the resistivity of $(TMTTF)_2 TaF_6$ under several pressures (from 1.5 GPa to 8 GPa). The external pressure was applied by using the CAC pressure generator, which can compress the sample with liquid pressure-transmitted medium in a Teflon cell-surrounded MgO gasket from six directions simultaneously, using an external automatic 250-ton load piston. The temperature range for the measurement was from 1.8 K to room temperature. The resistivity along the *a*-axis direction was measured by the four-probe method; the resistivity data were recorded on heating procedure by slow temperature control. (**b**) Resistivity versus temperature for $(TMTTF)_2 TaF_6$ (black lines) and $(TMTTF)_2 SbF_6$ (dash-dot lines). The resistivity of $(TMTTF)_2 SbF_6$ is reproduced by Ref. [9]. The ground states for both samples are CO (T_{CO} = 175 K for X = TaF_6 and 154 K for X = SbF_6) and AFM (anti-ferromagnetism, T_{AF} = 9 K for X = TaF_6 and 8 K for X = SbF_6). $(TMTTF)_2 TaF_6$ shows higher resistivity than $(TMTTF)_2 SbF_6$. (**c**) $\log \rho(T)$ versus $1/T$ plot. T_ρ and T_S are defined as points of the first slope change and the second change in $\log \rho(T)$ -$1/T$ plot.

At 5 GPa, the zero-resistivity is observed due to an occurrence of a pressure-induced superconductivity transition at 2.83 K. It should be noted that the value of resistivity (0.047 $\Omega \cdot$cm) at 300 K is one order higher than that of the SbF_6 salt and the zero-resistivity was observed using the CAC apparatus in $(TMTTF)_2 X$ series except for the X = SbF_6 salt [7–9]. Figure 4 displays the temperature-dependent resistivity from 5 GPa to 8 GPa at low temperatures (between 1.8 K and 10 K). The superconductivity phase exists in a quite short pressure region of $5 \leq P \leq 6$ GPa; the shape of the SC phase is completely different from the $(TMTTF)_2 SbF_6$ salt ($5.4 \leq P \leq 9$ GPa). The maximum T_C is 2.8 K at 5 GPa, the superconducting temperature shifts to a slightly lower temperature with increasing pressure, and then the SC state almost disappears at 6 GPa. Above 7 GPa, only metallic behavior is observed. By estimating the power of temperature (T) with $\rho(T) \sim T^\alpha$ between 6 GPa and 8 GPa, the α increases linearly as pressure increases and reaches ~1.5 at 8 GPa.
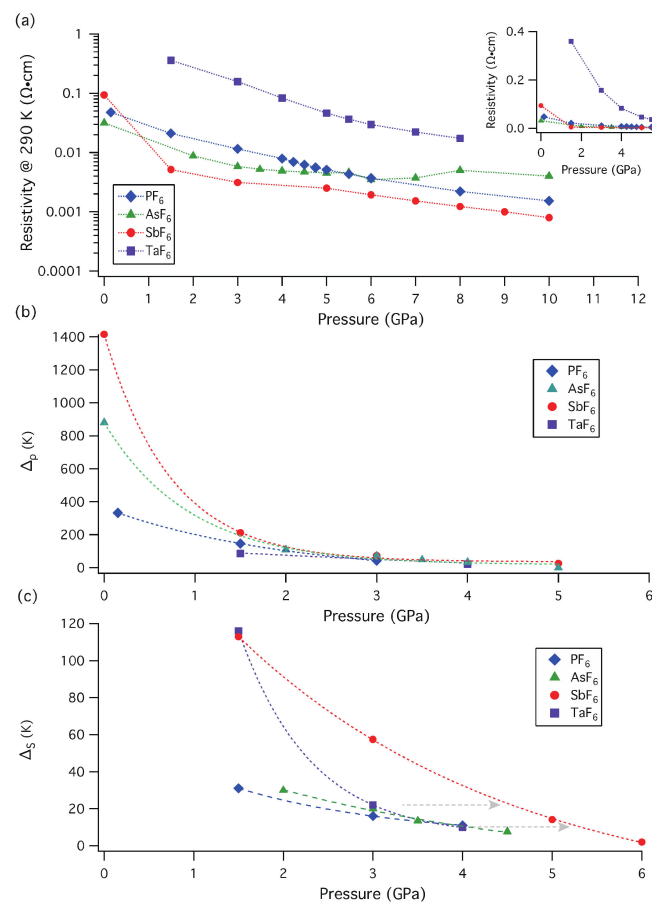
Figure 3. (**a**) Resistivity at 290 K versus pressure plots for (TMTTF)$_2$$X$ (X = PF$_6$, AsF$_6$, SbF$_6$, and TaF$_6$) obtained using the CAC pressure generator (single logarithmic plot). (Inset) Enlarged resistivity-pressure graphs below 6 GPa. Pressure-dependent activation energy (**b**) Δ_ρ and (**c**) Δ_S for (TMTTF)$_2$$X$ (X = PF$_6$, AsF$_6$, SbF$_6$, and TaF$_6$) obtained by fitting of log $\rho(T)$ vs $\frac{1}{T}$ plots. Dot lines are a guide for the eyes. The resistivities $\rho(T)$ along *a*-axis are regulated by the sample size at ambient pressure of 300 K. To compare with the data for (TMTTF)$_2$TaF$_6$, we reproduced the resistivity-pressure plot Δ_ρ and Δ_S for X = PF$_6$, AsF$_6$, and SbF$_6$ using references [7–9].
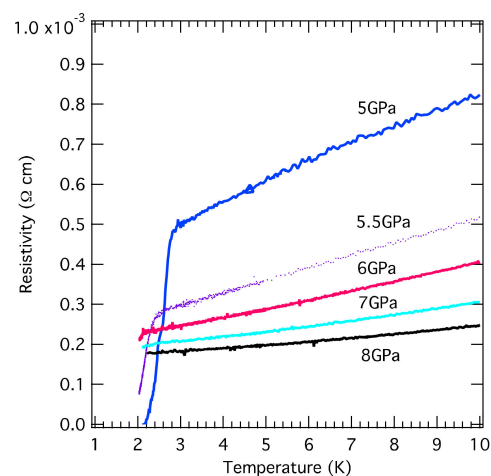

Figure 4. Temperature-dependent resistivity from 1.8 K to 10 K for (TMTTF)$_2$TaF$_6$ under various pressures. The lowest-achieving temperature is 1.8 K for the resistivity measurement using the CAC pressure generator. Superconducting behavior is observed around 2 K in the narrow pressure region, between 5 GPa and 6 GPa. Above 7 GPa, the superconducting state is not observed in the measured temperature range; the resistivity linearly increases as temperature increases.

The main physical parameters, maximum superconducting transition temperature T_C and the pressure P_C, activation energy Δ_S at 3 GPa, lattice parameters along the *a*-axis, volumes, and ground states at ambient pressure for $(TMTTF)_2X$ (PF_6, AsF_6, SbF_6, and TaF_6) are listed in Table 1. The *T-P* diagram of $(TMTTF)_2TaF_6$ based on the result of this resistivity measurement is described in Figure 5, in which the electron-correlation change is referred to in the data of $(TMTTF)_2PF_6$. This phase diagram is obtained by adjusting both pressure points of TaF_6 and the PF_6, where the maximum SC transition temperatures (T_C (PF_6) and T_C (TaF_6)) were recorded. The ground states of the TaF_6 salt vary in CO/AFM I -(SP)- SDW (C-SDW: commensurate spin density wave and I-SDW: incommensurate spin density wave) and SC as referred to in reports [1,2] and the previous studies [7–9]. In this case, the chemical pressure between the PF_6 and TaF_6 salts is roughly estimated as 0.75 GPa. Due to the fact that the ground state change at a lower pressure in the TaF_6 salt has not yet been proven, the pressure range on the lower pressure side of Figure 1 differs from that of this *T-P* phase diagram.

Table 1. Physical properties of $(TMTTF)_2X$ ($X = PF_6$, AsF_6 SbF_6, and TaF_6). T_{CO}, activation energies for Δ_S at 3 GPa, lattice parameters and volumes at ambient temperature, superconducting (SC) temperature T_C and the observed pressure, and ground states at low temperature (0 GPa). Δ_S, T_C, and pressure region for SC were obtained using resistivity measurements with the CAC pressure generator.

$(TMTTF)_2X$	T_{CO}	Activation Energy 3 GPa Δ_S [K]	Lattice Parameter a^* [Å]	V [Å^3] at Room Temperature *	Superconducting Temperature T_C [K]	Pressure at Maximum T_C [K] (Pressure Region for SC Phase) **	T_{SP} [K]	T_{AF} [K]
PF_6	70	16	7.172(11)	676.6	2.5	4.3 (4.0 ≤ P ≤ 5.0 GPa)	15	
AsF_6	102	17	7.1662(4)	686.15	2.6	5.0 (4.5 ≤ P ≤ 5.0 GPa)	14	
SbF_6	154	57	7.1796(11)	702.93	2.8	6.0, 9.0 (5.4 ≤ P ≤ 9.0 GPa)		8
TaF_6	175	22	7.1862(11)	706.52	2.8	5.0 (5.0 ≤ P ≤ 6.0 GPa)		9

* Lattice parameters and volumes refer to Ref. [28]. ** The temperature region for the resistivity measurement by the CAC was from 1.8 K to 300 K.

The emergence of the SC phase in the narrow pressure region for the TaF_6 salt is similar to those observed in the PF_6 and AsF_6 salts; however, the SC phase of the SbF_6 salt is observed over a wide pressure range (see Figure 5b). The reason is probably attributed to the difference in structural compression sensitivity corresponding to the dimensionality by applied pressure and thermal expansion upon cooling. The structural investigation and the DFT calculations indicated that pressure (~2.7 GPa) and a lower temperature increase two-dimensionality in $X = PF_6$ and SbF_6 [36,37]. It was reported that, in the structure of $(TMTTF)_2PF_6$ under high pressure, the space group $P\bar{1}$ remains up to 8 GPa and a pressure-induced structural transition (triclinic → monoclinic phase transition) occurs above 8.5 GPa [38]. The lattice *a* is dramatically compressed to approximately 12.5% and then the total unit cell volume shrinks by about 27.5% by external pressure up to 8 GPa. At the SC-appearing pressure (~4.3 GPa), the compressed lattice and volume where the SC can be observed are $a(PF_6)$ ~ 6.44 Å and $V(PF_6)$ ~ 540 Å^3, which are approximately 90% and 80% of the values at ambient pressure, respectively (see Table 1). Considering a simple estimation, since the actual pressure of the TaF_6 salt shifts by 1 GPa to the negative pressure side of that of the PF_6 salt, the volume of TaF_6 would be compressed to approximately 22.5% by $V(TaF_6)$ ~ 547 Å^3 to appear in the SC phase. Unfortunately, the bulk modulus and thermal expansion of $X = SbF_6$ and TaF_6 under high pressure are unknown. High pressure structural investigations in $X = SbF_6$ and TaF_6 are necessary to understand not only the origin of the high resistivity of TaF_6 but also the narrower SC phase compared to that of the SbF_6 salt.
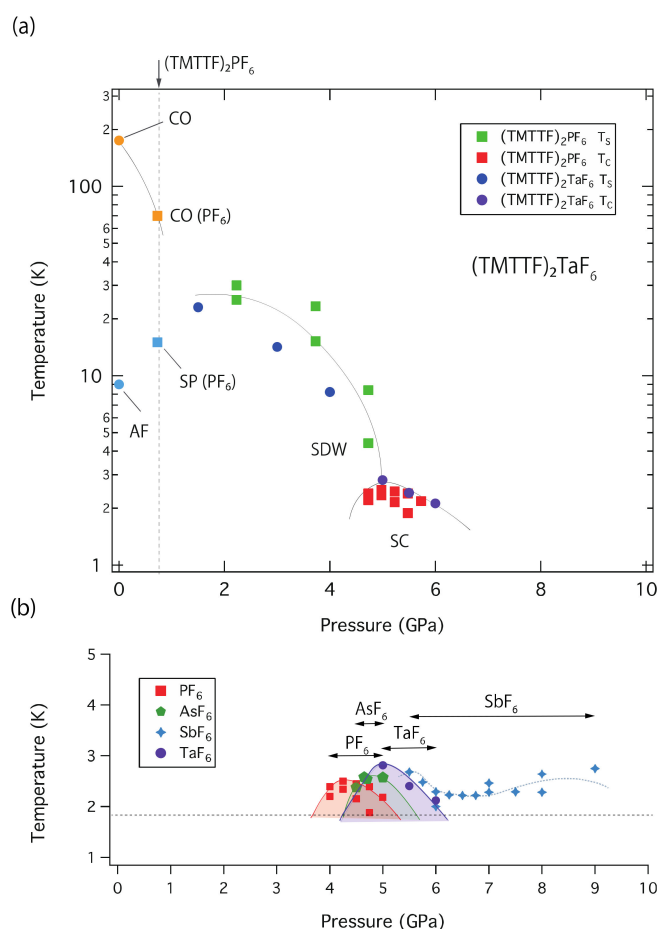
(a)

(b)

Figure 5. (**a**) Temperature-pressure (*T-P*) diagram of $(TMTTF)_2TaF_6$. The denoted ground states were obtained by referring to the electronic correlation of the PF_6 salt. The offset pressure between the SC (superconducting) phases of PF_6 and TaF_6 is estimated at 0.75 GPa by adjusting the pressures, at which the highest temperatures of the SC were observed in TaF_6 and PF_6 salts. (**b**) Superconducting transition temperature versus applied pressures in $(TMTTF)_2X$ for indicating the pressure region of superconducting phases observed by the resistivity measurements using the CAC pressure generator ($X = PF_6$ [7], AsF_6 [8], SbF_6 [9], and TaF_6 (this work)). A horizontal dot line indicates the lowest temperature limit of 1.8 K when high-pressure resistivity measurements were carried out by the CAC.

4. Conclusions

We measured resistivity for $(TMTTF)_2TaF_6$ under high pressure (up to 8 GPa) using a CAC pressure apparatus that can generate hydrostatic pressure. $(TMTTF)_2TaF_6$ has charge-ordering (T_{CO} = 175 K) and anti-ferromagnetic (T_{AF} = 9 K) states at ambient pressure. At 3 and 4 GPa, the growth of resistivity was observed at low temperatures due to spin-related transition; SDW (C-SDW and/or I-SDW) is predicted from our T-P phase diagram, as observed in $(TMTTF)_2X$ ($X = PF_6$, AsF_6, and SbF_6). With increasing applied pressure, a superconducting (SC) state appears at 5 GPa. The T_C of $(TMTTF)_2TaF_6$ records the highest SC temperature of 2.8 K (at 5 GPa) in the $(TMTTF)_2X$ series. However, the SC phase is observed in the short pressure region between 5 GPa and 6 GPa above ~2 K. From the results of high-pressure resistivity measurements with the CAC pressure generator for the Q1D organic conductor $(TMTTF)_2X$ ($X = PF_6$, AsF_6, SbF_6, and TaF_6), the generalized TMTCF *T-P* diagram could be extended by confirming the SC phase in TaF_6 salt with a negative offset pressure of ΔP~0.75 GPa when the pressures at maximum SC temperature were compared between the PF_6 and the TaF_6 salts. High-pressure X-ray structural measurement is future work required to reveal the different appearances of SC phase shapes between TaF_6 and SbF_6 salts under high pressure.

References

1. Jérome, D. The Physics of Organic Superconductors. *Science* **1991**, *252*, 1509–1514. [CrossRef] [PubMed]
2. Adachi, T.; Ojima, E.; Kato, K.; Kobayashi, H.; Miyazaki, T.; Tokumoto, M.; Kobayashi, A. Superconducting Transition of $(TMTTF)_2PF_6$ above 50 kbar [TMTTF = Tetramethyltetrathiafulvalene]. *J. Am. Chem. Soc.* **2000**, *122*, 3238–3239. [CrossRef]
3. Jaccard, D.; Wilhelm, H.; Jérome, D.; Moser, J.; Carcel, C.; Fabre, J.M. From spin-Peierls to superconductivity: $(TMTTF)_2PF_6$ under high pressure. *J. Phys. Condens. Matter* **2001**, *13*, L89–L95. [CrossRef]
4. Mori, H. Materials Viewpoint of Organic Superconductors. *J. Phys. Soc. Jpn.* **2006**, *75*, 051003. [CrossRef]
5. Dressel, M. Spin-charge separation in quasi one-dimensional organic conductors. *Naturwissenschaften* **2003**, *90*, 337–344. [CrossRef]
6. Ishiguro, T.; Yamaji, K.; Saito, G. *Organic Superconductors*, 2nd ed.; Fulde, P., Ed.; Springer Series in Solid-State Sciences 88; Springer: Berlin, Germany, 1998.
7. Araki, C.; Itoi, M.; Hedo, M.; Uwatoko, Y.; Mori, H. Electrical Resistivity of $(TMTTF)_2PF_6$ under High Pressure. *J. Phys. Soc. Jpn.* **2007**, *76*, 198–199. [CrossRef]
8. Itoi, M.; Kano, M.; Kurita, N.; Hedo, M.; Uwatoko, Y.; Nakamura, T. Pressure-Induced Superconductivity in the Quasi-One-Dimensional Organic Conductor $(TMTTF)_2AsF_6$. *J. Phys. Soc. Jpn.* **2007**, *76*, 053703. [CrossRef]
9. Itoi, M.; Araki, C.; Hedo, M.; Uwatoko, Y.; Nakamura, T. Anomalously Wide Superconducting Phase of One-Dimensional Organic Conductor $(TMTTF)_2SbF_6$. *J. Phys. Soc. Jpn.* **2008**, *77*, 23701. [CrossRef]
10. Kano, M.; Mori, H.; Matsubayashi, K.; Itoi, M.; Hedo, M.; Murphy, T.P.; Tozer, S.W.; Uwatoko, Y.; Nakamura, T. Anisotropy of Upper Critical Field in a One-Dimensional Organic System, $(TMTTF)_2PF_6$ under High Pressure. *J. Phys. Soc. Jpn.* **2012**, *81*, 024716. [CrossRef]
11. Balicas, L.; Behnia, K.; Kang, W.; Auban-Senzier, P.; Canadell, E.; Jérome, D.; Ribault, M.; Fabre, J.-M. $(TMTTF)_2Br$: The First Organic Superconductor in the $(TMTTF)_2X$ family. *Adv. Mater.* **1994**, *6*, 762–765. [CrossRef]
12. Hisano, M.; Nakamura, T.; Takahashi, T.; Saito, G. SDW wave number and charge localization in $(TMTTF)_2Br$: ^{1}H-NMR investigation. *Synth. Met.* **1999**, *103*, 2195. [CrossRef]
13. Hirose, S.; Liu, Y.; Kawamoto, A. ^{13}C NMR study of commensurate antiferromagnetism in $(TMTTF)_2Br$. *Phys. Rev. B* **2013**, *88*, 125121. [CrossRef]
14. Asada, M.; Nakamura, T. Magnetic resonance investigation for a possible antiferromagnetic subphase in $(TMTTF)_2Br$. *Phys. Rev. B* **2017**, *96*, 125120. [CrossRef]
15. Ishikawa, A.; Matsunaga, N.; Nomura, K.; Sasaki, T.; Nakamura, T.; Takahashi, T.; Saito, G. Electron correlation and two dimensionality in the spin-density-wave phase of $(TMTTF)_2Br$ under pressure. *Phys. Rev. B* **2003**, *67*, 212404. [CrossRef]
16. Lee, I.J.; Brown, S.E.; Naughton, M.J. Unconventional Superconductivity in a Quasi-One-Dimensional System $(TMTSF)_2X$. *J. Phys. Soc. Jpn.* **2006**, *75*, 051011. [CrossRef]
17. Yonezawa, S.; Kusaba, S.; Maeno, Y.; Auban-Senzier, P.; Pasquier, C.; Bechgaard, K.; Jérome, D. Anomalous In-Plane Anisotropy of the Onset of Superconductivity in $(TMTSF)_2ClO_4$. *Phys. Rev. Lett.* **2008**, *100*, 117002. [CrossRef]
18. Pratt, F.L.; Lancaster, T.; Blundell, S.J.; Baines, C. Low-Field Superconducting Phase of $(TMTSF)_2ClO_4$. *Phys. Rev. Lett.* **2013**, *110*, 107005. [CrossRef]
19. Nad, F.; Monceau, P. Dielectric Response of the Charge Ordered State in Quasi-One-Dimensional Organic Conductors. *J. Phys. Soc. Jpn.* **2006**, *75*, 051005. [CrossRef]
20. Köhler, B.; Rose, E.; Dumm, M.; Untereiner, G.; Dressel, M. Comprehensive transport study of anisotropy and ordering phenomena in quasi-one-dimensional $(TMTTF)_2X$ salts (X = PF_6, AsF_6, SbF_6, BF_4, ClO_4, ReO_4). *Phys. Rev. B* **2011**, *84*, 035124. [CrossRef]
21. Furukawa, K.; Sugiura, K.; Iwase, F.; Nakamura, T. Structural investigation of the spin-singlet phase in $(TMTTF)_2I$. *Phys. Rev. B* **2011**, *83*, 184419. [CrossRef]
22. Kitou, S.; Fujii, T.; Kawamoto, T.; Katayama, N.; Maki, S.; Nishibori, E.; Sugimoto, K.; Takata, M.; Nakamura, T.; Sawa, H. Successive Dimensional Transition in $(TMTTF)_2PF_6$ Revealed by Synchrotron X-ray Diffraction. *Phys. Rev. Lett.* **2017**, *119*, 065701. [CrossRef] [PubMed]

23. Kitou, S.; Zhang, L.; Nakamura, T.; Sawa, H. Complex changes in structural parameters hidden in the universal phase diagram of the quasi-one-dimensional organic conductors (TMTTF)$_2$X (X = NbF$_6$, AsF$_6$, PF$_6$, and Br). *Phys. Rev. B* **2021**, *103*, 184112. [CrossRef]

24. Nakamura, T. Possible Charge Ordering Patterns of the Paramagnetic Insulating States in (TMTTF)$_2$X. *J. Phys. Soc. Jpn.* **2003**, *72*, 213–216. [CrossRef]

25. Yoshimi, K.; Seo, H.; Ishibashi, S.; Brown, S.E. Tuning the Magnetic Dimensionality by Charge Ordering in the Molecular TMTTF Salts. *Phys. Rev. Lett.* **2012**, *108*, 096402. [CrossRef]

26. Yu, W.; Zhang, F.; Zamborszky, F.; Alavi, B.; Baur, A.; Merlic, C.A.; Brown, S.E. Electron-lattice coupling and broken symmetries of the molecular salt (TMTTF)$_2$SbF$_6$. *Phys. Rev. B* **2004**, *70*, 121101. [CrossRef]

27. Iwase, F.; Sugiura, K.; Furukawa, K.; Nakamura, T. ^{13}C NMR study of the magnetic properties of the quasi-one-dimensional conductor (TMTTF)$_2$SbF. *Phys. Rev. B* **2011**, *84*, 115140. [CrossRef]

28. Iwase, F.; Sugiura, K.; Furukawa, K.; Nakamura, T. Electronic Properties of a TMTTF-Family Salt, (TMTTF)$_2$TaF$_6$: New Member Located on the *Modified* Generalized Phase-Diagram. *J. Phys. Soc. Jpn.* **2009**, *78*, 104717. [CrossRef]

29. Dumm, M.; Loidl, A.; Fravel, B.W.; Starkey, K.P.; Montgomery, L.K.; Dressel, M. Electron spin resonance studies on the organic linear-chain compounds (TMTCF)$_2$X (C = S, Se; X = PF$_6$, AsF$_6$, ClO$_4$, Br). *Phys. Rev. B* **2000**, *61*, 511–521. [CrossRef]

30. Rösslhuber, R.; Rose, E.; Ivek, T.; Pustogow, A.; Breier, T.; Geiger, M.; Schrem, K.; Untereiner, G.; Dressel, M. Structural and Electronic Properties of (TMTTF)$_2$X Salts with Tetrahedral Anions. *Crystals* **2018**, *8*, 121. [CrossRef]

31. Dressel, M.; Dumm, M.; Knoblauch, T.; Masino, M. Comprehensive Optical Investigations of Charge Order in Organic Chain Compounds (TMTTF)$_2$X. *Crystals* **2012**, *2*, 528–578. [CrossRef]

32. Oka, Y.; Matsunaga, N.; Nomura, K.; Kawamoto, A.; Yamamoto, K.; Yakushi, K. Charge Order in (TMTTF)$_2$TaF$_6$ by Infrared Spectroscopy. *J. Phys. Soc. Jpn.* **2015**, *84*, 114709. [CrossRef]

33. Pustogow, A.; Dizdarevic, D.; Erfort, S.; Iakutkina, O.; Merkl, V.; Untereiner, G.; Dressel, M. Tuning Charge Order in (TMTTF)$_2$X by Partial Anion Substitution. *Crystals* **2021**, *11*, 1545. [CrossRef]

34. Nakamura, T.; Maeda, K. Competition electronic states of (TMTTF)$_2$MF$_6$: ESR investigations. *J. Phys. IV Fr.* **2004**, *114*, 123–124. [CrossRef]

35. Voloshenko, I.; Herter, M.; Beyer, R.; Pustogow, A.; Dressel, M. Pressure-dependent optical investigations of Fabre salts in the charge-ordered state. *J. Phys. Condens. Matter* **2017**, *29*, 115601. [CrossRef] [PubMed]

36. Rose, E.; Loose, C.; Kortus, J.; Pashkin, A.; Kuntscher, C.A.; Ebbinghaus, S.G.; Hanfland, M.; Lissner, F.; Schleid, T.; Dressel, M. Pressure-dependent structural and electronic properties of quasi-one-dimensional (TMTTF)$_2$PF$_6$. *J. Phys. Condens. Matter.* **2013**, *25*, 014006. [CrossRef] [PubMed]

37. Jacko, A.C.; Feldner, H.; Rose, E.; Lissner, F.; Dressel, M.; Valentí, R.; Jeschke, H.O. Electronic properties of Fabre charge-transfer salts under various temperature and pressure conditions. *Phys. Rev. B* **2013**, *87*, 155139. [CrossRef]

38. Pashkin, A.; Dressel, M.; Ebbinghaus, S.G.; Hanfland, M.; Kuntscher, C.A. Pressure-induced structural phase transition in the Bechgaard-Fabre salts. *Synth. Met.* **2009**, *159*, 2097–2100. [CrossRef]